Immunity, Vol. 13, 727–736, November, 2000, Copyright ©2000 by Cell Press

Crystal Structure and Ligand Binding Properties of the D1D2 Region of the Inhibitory Receptor LIR-1 (ILT2)

Tara L. Chapman,*§ Astrid P. Heikema,*† Anthony P. West, Jr.,* and Pamela J. Bjorkman*†‡
*Division of Biology 156-29 and
†Howard Hughes Medical Institute
California Institute of Technology
Pasadena, California 91125

Summary

LIR-1 is an inhibitory receptor that recognizes class I MHC molecules and the human cytomegalovirus class I homolog UL18. Here, we report the 2.1 Å resolution crystal structure of the ligand binding portion of LIR-1 (domains 1 and 2 [D1D2]) and localize the binding region for UL18. LIR-1 D1D2 is composed of two immunoglobulin-like domains arranged at an acute angle to form a bent structure resembling the structures of natural killer inhibitory receptors (KIRs). The LIR-1 binding site comprises a portion of D1 distant from the interdomain hinge region that constitutes the KIR binding site, consistent with differences in LIR-1 and KIR recognition properties and functions.

Introduction

Leukocyte immunoglobulin-like receptor-1 (LIR-1; also known as ILT2 [Samaridis and Colonna, 1997]) is a member of a family of immunoreceptors expressed on monocytes, B cells, dendritic cells, and subsets of natural killer (NK) and T cells (Borges et al., 1997; Colonna et al., 1997; Fanger et al., 1998). The LIR family comprises eight closely related human proteins sharing 63% to 84% sequence identity with LIR-1 (Borges et al., 1997). Based on functional assays (Colonna et al., 1997) and the presence of immunoreceptor tyrosine-based inhibitory motifs (ITIMs) in the cytoplasmic domains of LIR-1, -2, -3, -5, and -8 (Borges et al., 1997), LIR proteins are postulated to serve as inhibitory receptors, analogous to killer inhibitory receptors (KIRs) on human NK cells. KIRs recognize class I MHC molecules on target cells, thereby inhibiting activating signals delivered by NK activatory receptors and preventing NK-mediated lysis (Lanier, 1998). Class I MHC proteins are highly polymorphic within the human population, and individual KIRs show allele specificity in ligand binding (Lanier, 1998). Recognition of class I MHC molecules has also been demonstrated for LIR-1 and LIR-2, but each LIR protein binds to a broad range of classical and nonclassical MHC class I proteins (Colonna et al., 1997; Fanger et al., 1998; Lanier, 1998; Chapman et al., 1999; Navarro et al., 1999). In addition, LIR-1 recognizes UL18, a class I MHC homolog encoded by human cytomegalovirus (Cosman et al., 1997).

LIR and KIR proteins are members of the immunoglobulin superfamily (IgSF). The extracellular regions contain four (LIR-1, -2, -3, -4, -6a, -7, -8), three (p70 KIRs), or two (LIR-5, -6b, and p58 KIRs) IgSF domains (Colonna and Samaridis, 1995; Wagtmann et al., 1995; Borges et al., 1997). The first two domains (D1D2) of LIR-1 share ~37% amino acid sequence identity with the corresponding regions of p58 and p70 KIRs; however, the ligand recognition properties of LIR and KIR proteins differ. The binding site on LIR-1 for class I MHC molecules primarily involves D1 (Chapman et al., 1999), whereas the MHC class I binding site on p58 KIRs includes D1 and D2 residues in the vicinity of the interdomain hinge (Biassoni et al., 1997; Winter and Long, 1997; Winter et al., 1998; Boyington et al., 2000). In addition, LIR and KIR proteins bind to different regions of their class I MHC ligands. LIR-1 recognizes the relatively nonpolymorphic α3 domain of MHC class I molecules (Chapman et al., 1999), rationalizing the broad MHC class I binding specificity (Colonna et al., 1997; Cosman et al., 1997; Navarro et al., 1999), whereas p58 KIRs recognize a polymorphic region within the α1-α2 domain peptide binding region of MHC class I molecules (Lanier, 1998; Boyington et al., 2000), thus explaining the ability of individual KIRs to distinguish between MHC alleles. The broad binding specificity of LIR-1 includes recognition of UL18 (Cosman et al., 1997), which shares only ~25% sequence identity with classical MHC class I molecules (Beck and Barrell, 1988). In common with LIR-1/class I MHC interactions, the primary binding epitopes are LIR-1 D1 and the UL18 α3 domain (Chapman et al., 1999).

Here, we report the crystal structure and ligand binding site of a LIR-1 fragment (LIR-1 D1D2) analogous to the extracellular regions of p58 KIRs. We find that LIR-1 D1D2 is structurally similar to p58 KIRs but that it utilizes a different ligand binding surface. These results are discussed in light of the distinct functions of LIR and KIR family proteins.

Results

Crystal Structure of LIR-1 D1D2

LIR-1 D1D2 binds to UL18 and class I MHC proteins with the same binding affinity as the full-length extracellular region (Chapman et al., 1999). The crystal structure of LIR-1 D1D2 was determined in space group $P4_12_12$ to 2.1 Å resolution and in space group $P2_1$ to 3.8 Å resolution (Table 1). LIR-1 D1D2 consists of two tandem Ig-like domains that form a bent structure with an acute interdomain angle (Figure 1A). Both domains are primarily composed of β structure arranged into two antiparallel β sheets with a KIR-like folding topology (Figure 1B). Similar to KIR domains, the first β strand of each LIR-1 domain is shared between the β sheets, such that the strand A region pairs with strand B on one sheet and the A′ region pairs with strand G on the other sheet

‡To whom correspondence should be addressed (e-mail: bjorkman@caltech.edu).
§Present address: Department of Chemistry and Biochemistry, University of California, San Diego, California 92093.

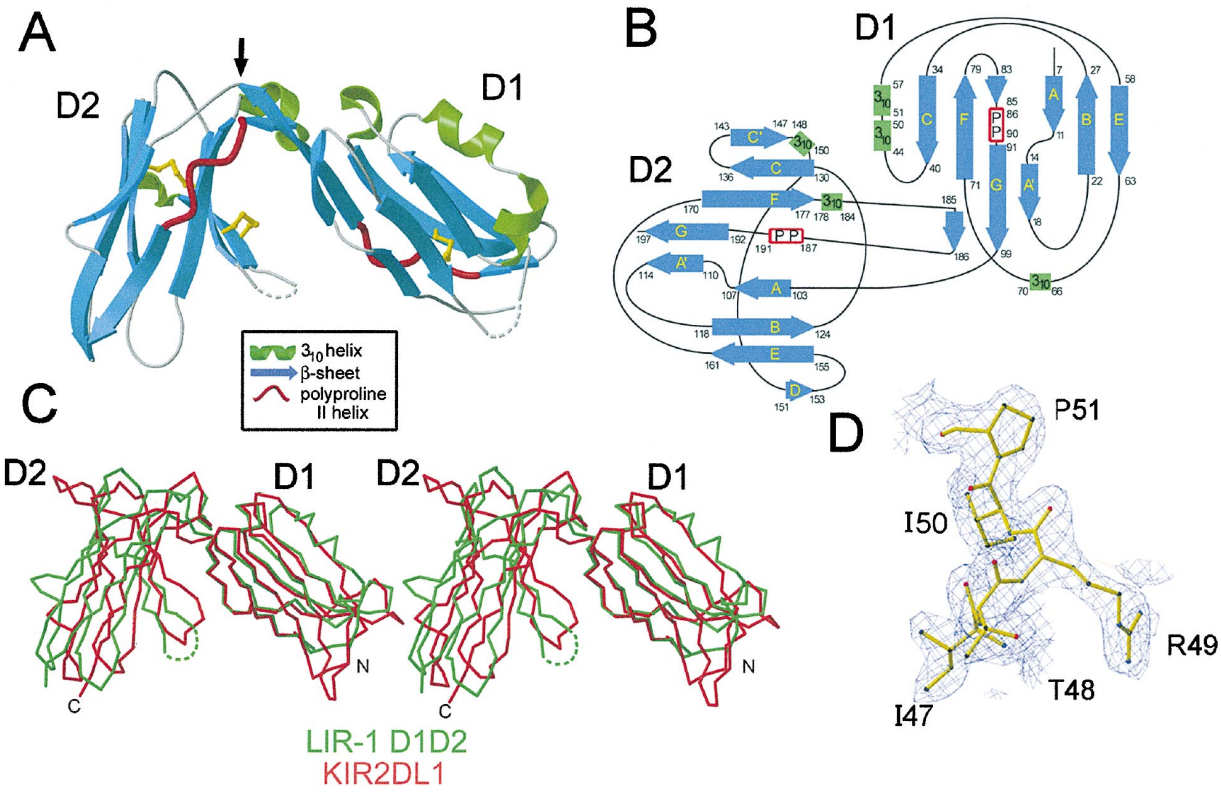

Figure 1. LIR-1 D1D2 Crystal Structure

(A) Ribbon diagram of the structure of LIR-1 D1D2. Disulfide bonds are shown in yellow, and dashed lines indicate disordered loops. Arrow indicates the location of the bond between residues 99 and 100, which can be proteolitically cleaved to generate stable fragments corresponding to D1 and D2 (Chapman et al., 1999).

(B) Topology diagram of LIR-1 D1D2. β strands are blue, 3_{10} helices are green, and polyproline type II helices are red.

(C) Stereoview of LIR-1 D1 (green) superimposed upon KIR2DL1 (Fan et al., 1997) (red). N and C termini of LIR-1 D1D2 are labeled. Cα atoms of the D1 domains of each structure were superimposed, illustrating the slight displacement of the D2 domains. Root mean square deviation (r.m.s.d) values for superpositions: 0.92 Å (71 Cα atoms) (LIR-1 D1 and KIR2DL1 D1), 1.25 Å (88 Cα atoms) (LIR-1 D2 and KIR2DL1 D2), 1.36 Å (67 Cα atoms) (LIR-1 D1 and LIR-1 D2).

(D) LIR-1 D1D2 model in the region of the D1 3_{10} helix superimposed on a 2.1 Å $2|F_{obs}| - |F_{calc}|$ annealed omit electron density map contoured at 1.0σ (map radius, 3.5 Å).

(Figures 1A and 1B). In LIR-1, KIR (Fan et al., 1997; Maenaka et al., 1999; Snyder et al., 1999), and some Fc receptor domains (Garman et al., 1998; Maxwell et al., 1999; Sondermann et al., 1999), the A to A′ strand switch is centered at a proline in the *cis* conformation (Pro12 in LIR-1 D1, Pro108 in LIR-1 D2).

LIR-1 D1 and D2 include helical regions intermixed with the β structure, some of which are not found in KIR or other IgSF domains (Figures 1A and 1B). Unlike KIR and Fc receptor domains, strand C′ in LIR-1 D1 is replaced by residues that display the internal hydrogen bonding pattern of a 3_{10} helix. This helical region is interrupted by a proline at position 51. In the corresponding region of D2, the N-terminal portion of the strand C′ region is preserved as a β strand, but the C-terminal portion includes one turn of a 3_{10} helix. Short regions of 3_{10} helix are also found in a loop between the E and F strands in D1 and between the F and G strands in D2. Another secondary structural element found in both LIR-1 domains is a polyproline II type helix, a left-handed helix characterized by a three residue repeat and phi, psi angles near –75°, 145° (Adzhubei and Sternberg, 1993). The polyproline II helices are located in the F-G loop, which contains a variation of the WSXWS sequence motif of hematopoietic receptors (Bazan, 1990) (RSESS in LIR-1 D1; WSLPS in LIR-1 D2). As also found in cytokine receptors (de Vos et al., 1992; Somers et al., 1994; Livnah et al., 1996; Bravo et al., 1998), KIRs (Fan et al., 1997; Maenaka et al., 1999; Snyder et al., 1999), and fibronectin III repeats (Huber et al., 1994), the nitrogen and side chain hydroxyls of serines in positions n and n + 3 hydrogen bond with the main chain of strand F. In the D2 region, Ser-186 and Ser-189 make hydrogen bonds with strand F, causing a protrusion of the region between the serines into the interface between D1 and D2.

The LIR-1 Interdomain Interface

Since a total of three independent views of LIR-1 D1D2 were obtained from analyses of two crystal forms, we can assess the degree to which the LIR-1 interdomain angle varies and compare the results to analyses of the KIR structures. Interdomain angles of 90°, 85°, and 84° were determined (see Experimental Procedures) from the single LIR-1 D1D2 molecule in the tetragonal crystal form and from the two D1D2 molecules in the monoclinic

Table 1. Data Collection and Refinement Statistics for LIR-1 D1D2

Space Group	$P4_12_12$	Space Group	$P2_1$
Unit cell dimensions (Å)	68.3, 68.3, 129.7	Unit cell dimensions (Å)	35.9, 103.9, 59.9, $\beta = 93.7°$
Data Collection		Data Collection	
Resolution	30–2.0	Resolution	30–3.8
Unique reflections	21555 (2112)	Unique reflections	4367 (379)
Redundancy	3.6 (3.5)	Redundancy	2.3 (2.2)
[a]Completeness (%)	99.5 (99.5)	[a]Completeness (%)	86 (84.5)
I/σI	18.8 (3.6)	I/σI	11.6 (5.3)
[b]R_{merge} (%)	6.0 (29.7)	[b]R_{merge} (%)	7.9 (16.1)
Refinement		Refinement	
Resolution (Å)	20–2.1	Resolution (Å)	20–3.8
Work reflections	17642	Work reflections	3622
Test reflections	900 (4.8%)	Test reflections	323 (7.4%)
[c]R_{cryst} (%)	21.3	[c]R_{cryst} (%)	30.6
[d]R_{free} (%)	24.2	[d]R_{free} (%)	38.4
Number of atoms		Number of atoms	
Protein	1513 (194 of 200 residues)	Protein	2998
Water	245		
Average B factor	29.1 Å^2	Average B factor	65.7 Å^2
Anisotropic B correction		Anisotropic B correction	
$B_{11} = B_{22} = -1.32$ Å^2, $B_{33} = 2.65$ Å^2		$B_{11} = 18.44$ Å^2, $B_{22} = 9.75$ Å^2, $B_{33} = -28.19$ Å^2, $B_{13} = 12.25$ Å^2	
Model geometry			
Rms deviations from ideal:			
bond lengths (Å)	0.005		
bond angles (deg)	1.4		
Ramachandran plot quality:			
most favored	91.6%		
additionally allowed	7.7%		
generously allowed	0.0%		
disallowed	0.6%		

[a] Completeness = (number of independent reflections)/total theoretical number.
[b] R_{merge} (I) = $(\Sigma|I(i) - <I(h)>|/\Sigma I(i))$, where I(i) is the *i*th observation of the intensity of the hkl reflection and <I> is the mean intensity from multiple measurements of the h,k,l reflection.
[c] R_{cryst} (F) = $\Sigma_h||F_{obs}(h)| - |F_{calc}(h)||/\Sigma_h|F_{obs}(h)|$, where $|F_{obs}(h)|$ and $|F_{calc}(h)|$ are the observed and calculated structure factor amplitudes for the h,k,l reflection.
[d] R_{free} is calculated over reflections in a test set not included in atomic refinement.

crystal form. Interdomain angles were measured as 60°, 70°, and 80° for KIR2DL1, KIR2DL3, and KIR2DL2, respectively (Fan et al., 1997; Maenaka et al., 1999; Snyder et al., 1999), and 81° and 85° for independent KIR2DL2 molecules in a KIR/class I MHC complex structure (Boyington et al., 2000). Thus, the LIR-1 D1D2 interdomain angle falls within the higher limits of the range of angles seen in KIR structures.

The domain interface between LIR-1 D1D2 is formed by interactions between the E-F loop and strand G regions of D1 with the F-G loop of D2 and the connecting region between D1 and D2 (G-A loop) (Figures 2 and 3). A total of 1245 Å^2 of accessible surface area is buried at the interdomain interface, compared to values of 919 Å^2 to 1076 Å^2 calculated for KIR structures (Fan et al., 1997; Maenaka et al., 1999; Snyder et al., 1999). Of the 13 residues involved in the LIR-1 D1D2 interdomain interaction (Figure 3), most are hydrophobic (Ala-70, Val-94, Val-95, Thr-96, Gly-97, and Ala-98 from D1, and Tyr-99, Tyr-183, Trp-185, Ser-186, and Leu-187 from D2). The hydrophobic core formed by interactions between these residues is likely to stabilize the interdomain angle. A majority of the interdomain interactions involve two aromatic residues, Tyr-183 and Trp-185, which together contribute 31% of the total buried surface area. Trp-185 is part of the WSXWS sequence motif within the F-G loop of D2.

We previously predicted that the LIR-1 extracellular region would form an extended structure without extensive interactions between domains, based upon the stability of isolated LIR-1 domains (Chapman et al., 1999). However, the ability to proteolyze LIR-1 D1D2 into stable fragments (residues 1–99 and 100–197) corresponding approximately to D1 and D2 (Chapman et al., 1999) can be accounted for by accessibility of the bond between residues 99 and 100 (Figure 1A) and interspersed hydrophilic residues at the D1D2 interface (Figure 2B).

Structural Predictions for LIR-1 D1-D4 and Other LIR Family Members

The significant sequence identities relating individual LIR-1 domains to each other (25%–44%) and LIR-1 to other LIR family members (63%–84%) (Figures 2A and 2B) suggest that the remaining LIR-1 domains and the domains in other LIR proteins will fold into tertiary structures similar to LIR-1 D1 and D2. To address whether the D1D2 interdomain interfaces of other LIR proteins are similar to the LIR-1 D1D2 interface, we compared

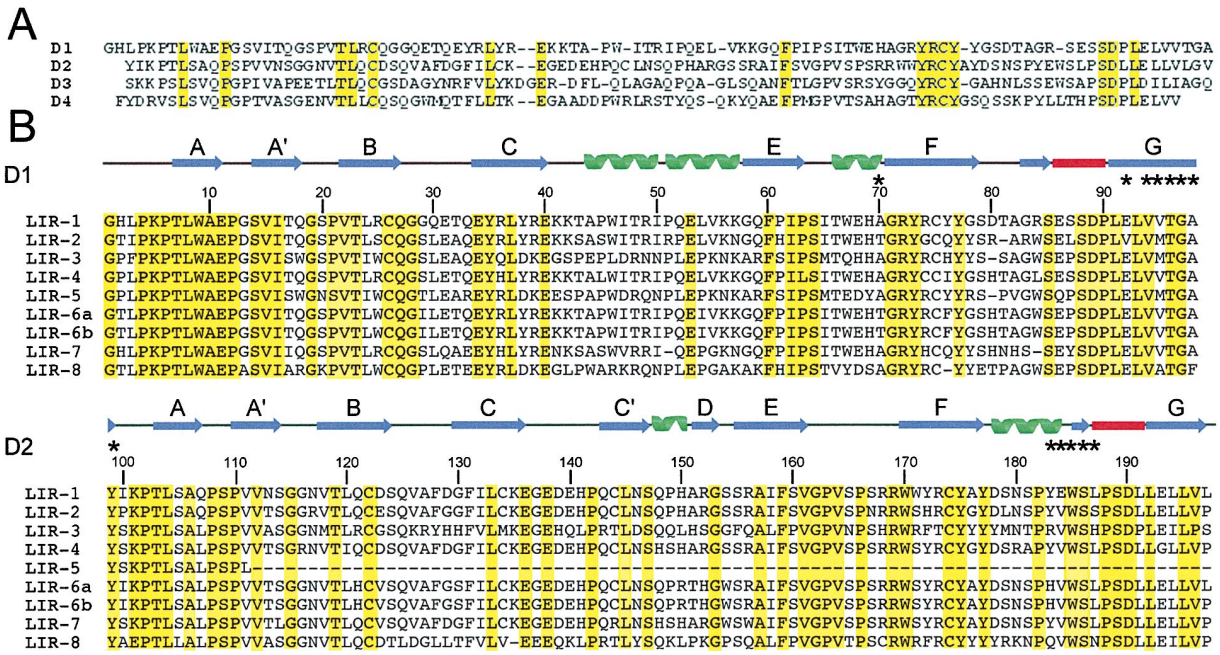

Figure 2. Sequence Alignments

Numbers refer to LIR-1. Locations of the secondary structural elements in the LIR-1 D1D2 structure are indicated above the sequences. Residues at the D1D2 interdomain interface that contribute more than 10 Å^2 of buried surface area to the interface are indicated with an asterisk and are yellow if they are identical in LIR-1 and the compared sequences. (A) Sequence alignment of LIR-1 domains. (B) Sequence alignment of D1D2 regions of LIR-1 and other LIR proteins.

the sequences of the LIR-1 D1D2 interface residues with their counterparts in other LIRs (Figure 2B). Six of the thirteen residues involved in the D1D2 interface are conserved in all members of the LIR family, including Trp-185 (Figure 2A). The remaining residues show some variability, but most changes are conservative. Thus, all LIR members are likely to share a common arrangement of D1 relative to D2.

The structures of entire extracellular regions of LIR-1 and the other LIR proteins will depend on the nature of the D2D3 and D3D4 interfaces. To determine if the D2D3 and D3D4 interfaces of LIR-1 are likely to be similar to the D1D2 interface, we examined the LIR-1 sequence (Figure 2A). Of the six residues within the strand G region of D1 that interacts with D2, three are conserved in the corresponding region of D2 that would interact with D3, and the others are conservatively substituted (Figure 3). In the D4 strand G region, one residue is conserved and four are conservatively substituted. Three of the five contact residues within the F-G loop of D2 are conserved in the corresponding region of D3, including D3 Trp-284, the counterpart of D2 Trp-185, a critical residue in the D1D2 interface. By contrast, the corresponding region of D4 does not contain a tryptophan and has only one residue conserved with the contact residues in D2. From this information, it appears more likely that D2 and D3 would interact in a manner analogous to D1 and D2 than would D3 and D4. In Figure 3, we present three possible models for the structure of the extracellular region of LIR-1. In the first, the D2D3 and D3D4 interfaces are modeled upon the D1D2 interface, forming a bent rod with a length of ~110 Å. The middle model shows a structure in which the D2D3 interface has the acute interdomain angle of D1D2 but D3 and D4 are oriented approximately parallel to each other to form a slightly longer molecule (125 Å). In the third model, both D3 and D4 are approximately parallel to their preceding domains, forming a LIR-1 extracellular region with the maximum possible length (140 Å).

Localization of the UL18 Binding Site on LIR-1

In order to identify candidate binding site residues, we compared the D1 sequences of LIR-1, which binds UL18 with nM affinity (Chapman et al., 1999), and LIR-2, which shows no detectable binding to cell surface UL18 when expressed as an Fc fusion protein (Borges et al., 1997). Solvent exposed residues that differ between the LIR-1 and LIR-2 sequences were considered candidate binding site residues, and their involvement in binding UL18 was investigated by determining the affinities of site-directed mutants of LIR-1 and LIR-2 D1D2 proteins. All proteins migrated in the expected position on a gel filtration column, and correct folding for mutants that displayed affinities for UL18 that were different from wild-type was verified by circular dichroism analyses (data not shown).

LIR-1 residues were introduced into LIR-2 in an effort to confer UL18 binding activity upon LIR-2. A biosensor-based assay was used to compare the binding of UL18 to the D1D2 regions of wild-type LIR-1 and LIR-2 and the LIR-2 mutants (Figure 4). Wild-type LIR-1 D1D2 binds to UL18 with an equilibrium dissociation constant (K_D) of ~2 nM, as compared to ~12 μM for LIR-2 D1D2 (Figures 4A and 4B). Substitution of LIR-2 residues Gln-76, Arg-80, and Trp-83 with their LIR-1 counterparts (LIR-2 mutant Q76Y/R80D/W83R) resulted in a ~10-fold

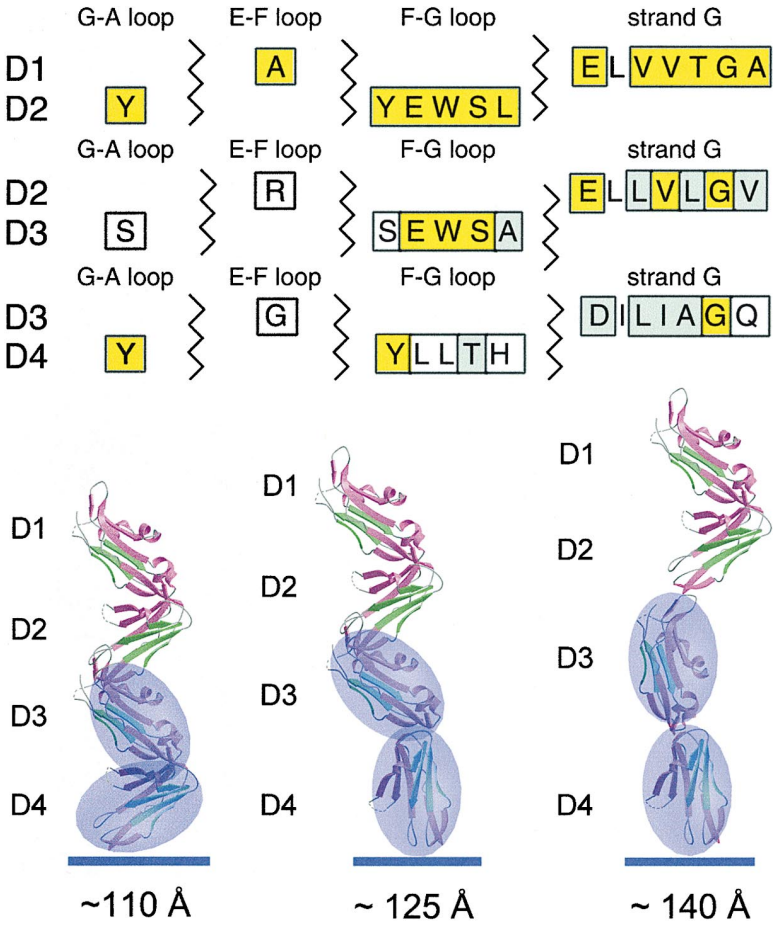

Figure 3. Hypothetical Models for the Structure of the LIR-1 Extracellular Region (D1-D4)

(A) Sequences of regions in D1 and D2 that are involved in the D1D2 interface are shown with residues contributing more than 10 Å^2 of buried surface area indicated in yellow boxes. Sequences of the counterpart regions in the other LIR-1 domains are shown with boxes around residues corresponding to D1D2 interface residues with conserved residues in yellow and chemically similar residues in green.

(B) Possible structures for the extracellular region of LIR-1. Approximate lengths of each model are indicated below its structure. The model on the left assumes all interfaces resemble the D1D2 interface and was constructed as follows: D1 of a D1D2 molecule was aligned on D2 and the position of the D2 domain of the aligned molecule was assigned as D3. D1 of a D1D2 molecule was then aligned on the model for D3, and the position of the D2 domain of the aligned molecule was assigned as D4. The middle model assumes that only the D2D3 interface resembles the D1D2 interface and was constructed following the procedure for the left model, except that the modeled D4 domain was positioned with its long axis roughly parallel to the long axis of the LIR-1 extracellular region. The model on the right assumes that D3 and D4 are both oriented approximately parallel to the long axis of the LIR-1 extracellular region.

increased binding affinity for UL18. Substitution of LIR-2 residues 29 and 30 (LIR-2 mutant S29G/L30Q) had no effect on the binding affinity for UL18. A composite mutant containing all five substitutions (Q76Y/R80D/W83R/S29G/L30Q) bound to UL18 with approximately the same affinity as the Q76Y/R80D/W83R mutant, confirming that substitution of LIR-2 residues 76, 80, and/or 83 with their LIR-1 counterparts increases the binding affinity for UL18 (Figure 4A).

In order to confirm the involvement of the LIR-1 counterparts of LIR-2 residues 76, 80, and/or 83 (LIR-1 residues 76, 80, and 84) in binding UL18, we examined the effects of changing these and nearby residues in LIR-1 D1D2. Alanine substitutions were introduced to make the LIR-1 mutant Y76A/D80A/R84A, which bound to UL18 with an ~20-fold reduced affinity compared with wild-type LIR-1 D1D2 (Figure 4C; Table 2). Consistent with the LIR-2 mutagenesis results, we found no effect on UL18 binding affinity when LIR-1 residues 29 and 30 were changed (LIR-1 mutant G29A/Q30A) (Figure 4D). The combined mutant (LIR-1 Y76A/D80A/R84A/G29A/Q30A) (Figure 4E) showed an ~20-fold reduction in UL18 binding affinity compared with wild-type LIR-1 D1D2, again demonstrating the involvement of LIR-1 residues Tyr-76, Asp-80, and/or Arg-84 in the binding site for UL18. Using the crystal structure of LIR-1 D1D2, we identified solvent exposed residues in the vicinity of residues 76, 80 and 84 and constructed additional LIR-1 D1D2 mutants. We found that mutation of Tyr-38 (LIR-1 mutant Y38A) resulted in an ~18-fold reduction in UL18 binding affinity (Figure 4F), whereas substitution of residues 36, 40, 41, 48, 49, 52, 53, and 74 resulted in proteins that bound to UL18 without significantly altered affinities (Table 2). The residues implicated in UL18 binding (Tyr-38 and one or more of Tyr-76, Asp-80, and Arg-84) are indicated on the LIR-1 D1D2 structure in Figure 5A. The residues cluster on the N-terminal end of the A′CC′FG face of the D1 domain in an area distant from the D1D2 linker region that contacts MHC class I molecules in KIRs (Biassoni et al., 1997; Winter and Long, 1997; Vales-Gomez et al., 1998; Winter et al., 1998; Boyington et al., 2000) (Figure 5B). To verify that the LIR-1 and KIR binding sites are different, we mutated LIR-1 residues that correspond to KIR residues at the binding site for MHC class I molecules. The LIR-1 mutants K42A/T43A and N180A show wild-type binding affinity for UL18, whereas substitution of KIR2DL2 residue 44 (the counterpart of LIR-1 residue 42) greatly reduces the binding affinity for MHC class I molecules (Winter et al., 1998; Boyington et al., 2000).

In both crystal forms of LIR-1 D1D2, the region that was identified as the UL18 binding site is involved in a crystal contact with another D1D2 protein. In the $P2_1$ crystals, the two molecules in the asymmetric unit are related by approximate 2-fold symmetry and are oriented such that the N-terminal end of the A′CC′FG face

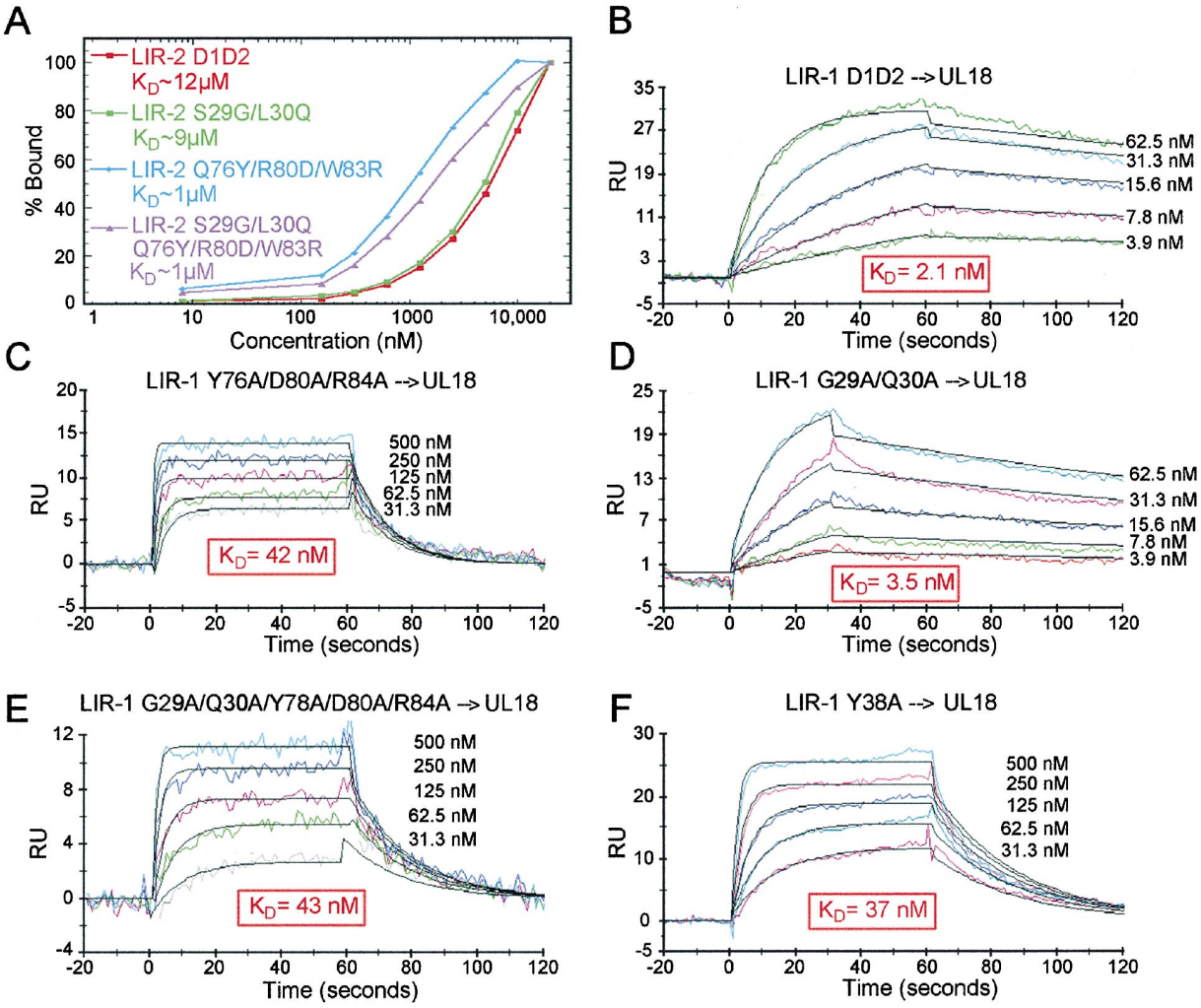

Figure 4. Biosensor Analyses of UL18 Binding to LIR-1 D1D2, LIR-2 D1D2, LIR-1, and LIR-2 Mutants

(A) Wild-type and mutant LIR-2 proteins analyzed using an equilibrium-based approach. Plot shows the percent bound (normalized equilibrium binding response [R_{eq}])versus the log of concentration of the indicated proteins. Derived K_D values are approximate because binding is not saturated at the highest concentration of protein possible to achieve, given the tendency of LIR-2 proteins to aggregate at high concentrations. (B–F) Sensorgrams (thick colored lines) from kinetics-based binding experiments overlaid with the calculated response (thin black lines) derived using a 1:1 binding model. In each panel, the injected protein is indicated in front of an arrow pointing to the immobilized protein. One representative set of injections from experiments performed in triplicate is shown for each interaction (analyses from triplicate experiments reported in Table 1).

in domain 1 contacts the same surface on the second molecule. This contact buries a total of ~870 Å^2 of accessible surface area, compared with an average of 570 Å^2 total surface area buried in nonspecific crystal contacts (Janin, 1997). The same interaction is present in the $P4_12_12$ crystals, in this case involving two molecules related by a crystallographic 2-fold and burying a total solvent accessible area of 810 Å^2. LIR-1 binds to UL18 with 1:1 stoichiometry (Chapman et al., 1999), suggesting that the crystallographically observed dimers are not relevant for ligand binding. However, the observation of an extensive interface involving the region of D1 identified as the UL18 binding site demonstrates that this surface has features favorable for protein–protein interactions and is therefore utilized both for crystal packing and ligand binding.

Discussion

Here, we report the crystal structure and ligand binding site of the first two domains of LIR-1, a monocyte, macrophage, and dendritic cell inhibitory receptor related to NK cell KIRs (Borges et al., 1997; Colonna et al., 1997; Cosman et al., 1997; Fanger et al., 1998). LIR-1 D1D2 consists of two IgSF domains that include more helical structure than generally found in such domains but otherwise bear a close resemblance to the structures of KIR domains (Figure 1C). Like KIR domains, the LIR-1 D1 and D2 domains meet at an acute angle to form an interface involving the D1 to D2 connecting region, and sections including the D1 strand E to F loop, D1 strand G, and the strand F to G loop in D2. Because of the high degree of identity shared between LIR family members

Table 2. Biosensor Analyses of UL18 Binding to LIR-1 D1D2, LIR-2 D1D2, LIR-1, and LIR-2 Mutants

Wild-Type or Mutant LIR-2 D1D2 → UL18		UL18 → Wild-Type or Mutant LIR-2 D1D2	
	K_D (μM)		K_D (μM)
LIR-2 D1D2 → UL18	~14	UL18 → LIR-2 D1D2	~12
LIR-2 S29G/L30Q → UL18	~10	UL18 → LIR-2 S29G/L30Q	~9
LIR-2 Q76Y/R80D/W83R → UL18	~0.5	UL18 → LIR-2 Q76Y/R80D/W83R	~1
LIR-2 S29G/L30Q/Q76Y R80D/W83R → UL18	~1	UL18 → LIR-2 S29G/L30Q Q76Y/R80D/W83R	~1

Wild-Type or Mutant LIR-1 D1D2 → UL18			
	K_D (nM)	k_a ($sec^{-1}M^{-1}$)	k_d (sec^{-1})
wt D1D2 → UL18	2.1 ± 0.6	(1.4 ± 0.2) × 10^6	(2.8 ± 0.4) × 10^{-3}
G29A/Q30A → UL18	3.5 ± 0.6	(8.6 ± 1) × 10^5	(2.9 ± 0.1) × 10^{-3}
R36A → UL18	3.3 ± 1	(1.4 ± 1) × 10^6	(4.6 ± 0.1) × 10^{-3}
E40A/K41A → UL18	1.6 ± 0.7	(3.1 ± 0.1) × 10^6	(5.1 ± 0.3) × 10^{-3}
K42A/T43A → UL18	1.2 ± 2	(1.5 ± 0.3) × 10^6	(1.8 ± 0.1) × 10^{-3}
T48A/R49A → UL18	2.4 ± 0.7	(1.5 ± 0.6) × 10^6	(3.6 ± 0.1) × 10^{-3}
Q52A/E53A → UL18	2.9 ± 0.7	(1.3 ± 0.1) × 10^6	(3.7 ± 0.5) × 10^{-3}
R74A → UL18	1.3 ± 1	(3.0 ± 2) × 10^6	(3.8 ± 0.4) × 10^{-3}
N180A → UL18	2.4 ± 0.8	(2.1 ± 0.2) × 10^6	(5.0 ± 0.5) × 10^{-3}
Y76A/D80A/R84A → UL18	42 ± 1.4	(1.3 ± 0.5) × 10^6	(5.3 ± 0.9) × 10^{-2}
G29A/Q30A/Y76A/D80A/R84A → UL18	43 ± 2.5	(1.4 ± 1.4) × 10^6	(6.0 ± 0.1) × 10^{-2}
Y38A → UL18	37 ± 1	(1.5 ± 0.3) × 10^6	(5.6 ± 0.6) × 10^{-2}

The injected protein is indicated in front of an arrow pointing to the immobilized protein. When kinetic constants (k_a and k_d) are reported, the binding data were fit to a 1:1 binding model, and the K_D was determined as k_d/k_a. K_Ds were determined from at least three independent measurements, and the numbers after the ± sign represent standard deviations. When no kinetic constants are reported, the K_D was determined from equilibrium binding data fit to a 1:1 binding model. Due to the tendency of LIR-2 D1D2 and LIR-2 D1D2 to aggregate at high concentrations, the highest concentration used was 20 μM, which was not sufficient to saturate binding; thus, the K_D values for LIR-1 binding to class I molecules are approximate.

(Borges et al., 1997) (Figure 2B), the LIR-1 D1D2 structure can be used as a first-order model for the structures of other LIR proteins.

We used site directed mutagenesis to identify residues that contribute to the LIR-1 interaction with UL18, a viral class I MHC homolog. Substitutions that affected the affinity between LIR-1 D1D2 and UL18 mapped to A′CC′FG face of the D1 domain, in a region distant from the MHC class I binding site on KIRs, which involves residues from D1 and D2 that cluster near the interdomain hinge (Biassoni et al., 1997; Winter and Long, 1997; Vales-Gomez et al., 1998; Winter et al., 1998; Boyington et al., 2000). Because the affinity of LIR-1 for class I MHC proteins is much lower than for UL18, we were unable to derive accurate affinities for the binding of the LIR-1 and LIR-2 mutants to class I molecules. However, since LIR-1 recognition of class I MHC proteins and UL18 shares common features (i.e., the LIR-1/UL18 and LIR-1/class I MHC interactions both primarily involve the LIR-1 D1 domain and the α3 domain of UL18 or class I proteins (Chapman et al., 1999)), it is possible that the LIR-1 binding site for class I proteins will also involve the region identified as the UL18 binding site.

Many of the features of the LIR-1 D1D2 and KIR structures are also found in the structures of Fc receptors such as FcεRI (Garman et al., 1998), the high-affinity receptor for IgE, and in FcγRIIa (Sondermann et al., 1999) and FcγRIIb (Maxwell et al., 1999), low-affinity receptors for IgG. These Fc receptors each contain two IgSF domains related by interdomain hinge angles slightly more acute than the 60°–85° angles observed in KIR structures (Fan et al., 1997; Maenaka et al., 1999; Snyder et al., 1999). Although the hinge angles are all acute, the domain positions in the Fc receptor structures are reversed from those observed in the LIR-1 and KIR structures, such that the D1 domains are located on opposite sides of D2 (Garman et al., 1998; Maxwell et al., 1999; Sondermann et al., 1999). Despite this difference, the ligand binding sites in the FcεRI and FcγRII proteins are located at the D1D2 hinge region (Garman et al., 1998; Sondermann et al., 2000), as also seen in KIRs (Biassoni et al., 1997; Winter and Long, 1997; Vales-Gomez et al., 1998; Winter et al., 1998; Boyington et al., 2000). By contrast, another two-domain IgSF family member, the Fc receptor for IgA (FcαR), shows different ligand binding properties. FcαR shares 35%–40% sequence identity with LIR and KIR proteins, compared with only ~20% with the other tandem IgSF domain Fc receptors (Wines et al., 1999). Site directed mutagenesis results mapped onto a homology based model of FcαR suggest the ligand binding site is located in a region analogous to the LIR-1 binding site (Wines et al., 1999). Thus, within the family of proteins containing IgSF domains related by an acute angle, different surfaces within a similar overall structure are utilized for ligand recognition.

The results reported here illustrate the versatility of recognition properties of immune system members of the IgSF and further demonstrate the distinctions between the LIR and KIR families of inhibitory receptors. Of the LIR proteins, only LIR-1 and LIR-2 show detectable binding to class I MHC molecules (Borges et al., 1997; Colonna et al., 1998). Ligands for LIR-3 through LIR-8 have not yet been identified. The structure of LIR-1 D1D2 and information about its binding site will facilitate functional comparisons with other LIR family members as information about ligand recognition by other LIR proteins becomes available.

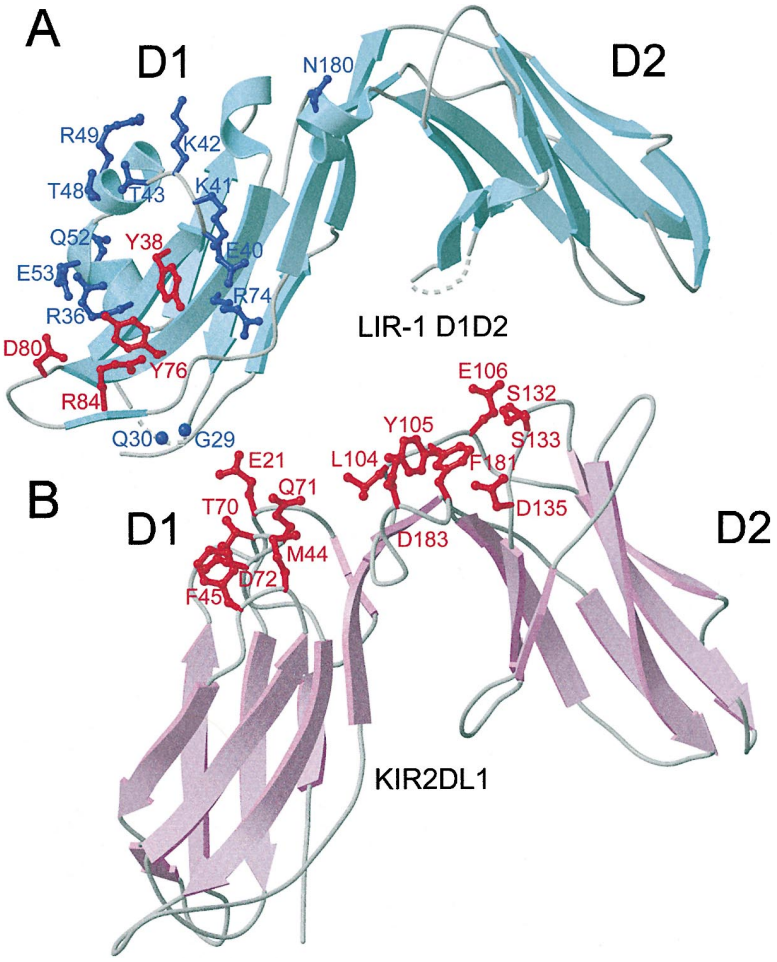

Figure 5. Comparison of Ligand Binding Sites on LIR-1 D1D2 and KIR2DL1

(A) Residues altered by site-directed mutagenesis are highlighted on a ribbon diagram of the LIR-1 D1D2 structure. Alteration of residues indicated in red resulted in changes in the affinity of LIR-1 D1D2 or LIR-2 D1D2 for UL18 (Table 2). Alteration of residues indicated in blue had no significant effect on the binding affinity.

(B) Residues contributing to the KIR binding site for class I MHC molecules (Biassoni et al., 1997; Winter and Long, 1997; Vales-Gomez et al., 1998; Winter et al., 1998; Boyington et al., 2000) are highlighted on the structure of KIR2DL1 (Fan et al., 1997).

Experimental Procedures

Protein Expression and Characterization

LIR-1 D1D2 and LIR-2 D1D2 (an initial methionine plus residues 1–197 of the mature protein) were expressed in *E. coli* strain BL21(DE3)pLysS and refolded from insoluble inclusion bodies as previously described (Chapman et al., 1999). Renatured protein was purified by gel filtration using a Superdex 200 26/60 column (Pharmacia). The N-terminal sequence of purified LIR-1 D1D2 was GHLPKPTLWAE (data not shown); thus, the methionine residue added to allow production in *E. coli* was lost. Site directed mutations were introduced into LIR-1 and LIR-2 using a QuikChange site-directed mutagenesis kit (Stratagene), and mutant proteins were expressed and purified following the procedure established for wild-type LIR-1 D1D2 (Chapman et al., 1999).

An AVIV 62A DS spectropolarimeter equipped with a thermoelectric cell holder was used for circular dichroism measurements. Wavelength scans and thermal denaturation curves were obtained from 10 μM solutions of wild-type or mutant LIR-1 D1D2 and LIR-2 D1D2 in 5 mM phosphate (pH 7) as described (Chapman et al., 1999).

Crystallization, Data Collection, and Processing

Crystals of LIR-1 D1D2 were grown at 22°C in 1:1 hanging drops containing D1D2 (8 mg/mL), 0.7 M potassium sodium tartrate, and 0.1 M Tris chloride (pH 8.5). Single crystals were transferred to a cryprotectant containing 20% ethylene glycol prior to data collection. The crystals belong to the tetragonal space group $P4_12_12$ (a = 68.3 Å, b = 68.3 Å, c = 129.7 Å; one molecule per asymmetric unit) and diffract to 2.1 Å resolution. Data were collected at −150°C from a single $P4_12_12$ crystal using a Quantum CCD Research detector at the Stanford Synchrotron Radiation Laboratory beamline 9–2 (λ = 1.000 Å). A second D1D2 crystal form was grown in 12% PEG 2000, 5% 2-methyl-2–4-pentanediol (MPD), 0.1 M MES (pH 6.0) and cryopreserved in a solution containing 20% MPD. These crystals (space group $P2_1$; a = 35.9 Å, b = 103.9 Å, c = 59.9 Å, β = 93.8°) diffract to 3.8 Å resolution and have two molecules per asymmetric unit. Data were collected at −150°C from a single $P2_1$ crystal using an R-AXIS IV mounted on a Rigaku RU-200 rotating anode generator (λ = 1.54 Å). Data were processed and scaled using DENZO and SCALEPACK (Otwinowski and Minor, 1997).

Structure Solution, Refinement, and Analysis

The structure for the $P4_12_12$ crystal form was determined by molecular replacement using AmoRe (Navaza, 1994). The 1.7 Å structure of KIR2DL1 (Fan et al., 1997) (PDB code 1NKR) (nonconserved side chains truncated to alanine and residues 1–6, 54–59 and 80–91 omitted) was used as a search model. D2 was first located (correlation coefficient: 34.1%; R factor of 52.3%). D1 was then found in a rotation and translation function in which D2 was fixed (correlation coefficient for D1 and D2: 41.8%; R factor of 49.0%). Rigid body refinement (20–4 Å) resulted in an R_{cryst} of 52.1% (R_{free} = 48.3%). Solvent-flattened maps calculated to 3.0 Å were used for initial rebuilding. Anisotropy and bulk solvent corrections were applied, and the model was refined (20–2.1 Å) using individual temperature (B) factors with CNS (Brünger et al., 1998). Residues at the N and C terminus of the fragment (1 and 199–200) and within two loops (30–31 and 138–140) are not seen in the electron density and were omitted from the model, and side chains for residues 2, 86, 141, and 143 are disordered. Disulfide bonds are found between cysteines 26 and 75, 122 and 174, and 134 and 144. The structure of the $P2_1$ crystal form was determined by molecular replacement (Navaza,

1994) using the refined LIR-1 D1D2 structure as a search model. Both domains D1D2 were used concurrently, but the angle between domains was not constrained. The top rotation function (20–3.8 Å) peak for domain 1 yielded a translation function (8–3.8 Å) solution (correlation coefficient: 31.7%; R factor of 51.5%), the top rotation function (20–3.8 Å) peak for domains 1 and 2 yielded a translation function (8–3.8 Å) solution (correlation coefficient: 43.8%; R factor of 47.7%). Rigid body refinement (20–3.8 Å) followed by group temperature (B) factor refinement using CNS (Brünger et al., 1998) resulted in an R_{cryst} of 30.6% and an R_{free} of 38.4%.

For analyses of interdomain angles, contacts, and buried surface areas, D1 was defined as residues 1–98 and D2 was defined as residues 99–198, following the structure-based definition of KIR2DL1 domain boundaries (Fan et al., 1997). Interdomain contact residues were defined as residues within 3.6 Å of the partner domain and identified using CONTACT (CCP4, 1994). Buried surface areas were calculated using SURFACE (CCP4, 1994) with a 1.4 Å probe radius. Interdomain angles were calculated by determining the angle between the long axes of adjacent domains, approximated by ellipsoids calculated from the coordinates using the program Dom_angle (Su et al., 1998).

Figures 1, 3, and 5 were made with Molscript (Kraulis, 1991) and Raster3D (Merritt and Murphy, 1994).

Biosensor-Based Affinity Measurements

A Biacore 2000 biosensor system (Pharmacia LKB Biotechnology) was used to determine binding affinities. Samples were purified by size exclusion chromatography to minimize the signal resulting from aggregated protein. Binding between a molecule coupled to a biosensor chip and a second molecule injected over the chip results in changes in the surface plasmon resonance signal that are read out in real time as resonance units (RU) (Karlsson and Fält, 1997). Proteins were covalently immobilized at pH 5.5 on a CM5 chip (Pharmacia LKB Biotechnology) using standard amine coupling chemistry as described in the Biacore manual. Samples were injected at room temperature in 50 mM PIPES (pH 7.0), 150 mM NaCl, and 0.005% Biacore surfactant P20. All injections were followed by an identical injection onto a mock-coupled flowcell.

Binding interactions between UL18 and LIR-1 proteins were assayed using short injection times (2–4 min) with fast flow rates (100 μl/min) over biosensor chips coupled to low densities (300 RU) (kinetics-based approach) to minimize mass transport effects upon the kinetics of the binding reactions (Karlsson and Fält, 1997). Kinetic constants were derived from sensorgram data using global fitting of the association and dissociation phases of all curves in the working set using BIAevaluation version 3.0. Sensorgrams were fit to a binding model that assumes a single class of noninteracting binding sites in a 1:1 binding interaction. K_D's were derived from the ratios of rate constants (k_a and k_d) as $K_D = k_d/k_a$.

Binding interactions between UL18 and LIR-2 proteins were assayed using an equilibrium-based approach that is not affected by mass transport effects. For these experiments, we used slow flow rates (5 μl/min) over biosensor chips coupled to high densities (1500–2000 RU). The response was measured 10 s after the start of the injection, and K_D's were derived by nonlinear regression analysis of plots of R_{eq} (the equilibrium binding response) versus the log of the injected protein concentration, and the data were fit to a 1:1 binding model as described (Vaughn and Bjorkman, 1997). A previous comparison of the kinetics-based versus equilibrium-based methods for determining K_D's demonstrated that both methods yielded comparable values for the same binding interaction (Lebrón et al., 1998).

Acknowledgments

We thank Z. Hamburger, B. Willcox, and C. O'Callaghan for assistance with crystallographic software and many helpful discussions, and D. Cosman and members of the Bjorkman lab for critical reading of the manuscript. This work was supported by a grant from the Arthritis Foundation (P. J. B.). Atomic coordinates have been deposited in the Protein Data Bank under accession code 1GOX.

Received August 15, 2000; revised October 11, 2000.

References

Adzhubei, A.A., and Sternberg, M.J.E. (1993). Left-handed polyproline II helices commonly occur in globular proteins. J. Mol. Biol. *229*, 472–493.

Bazan, J.F. (1990). Structural design and molecular evolution of a cytokine receptor superfamily. Proc. Natl. Acad. Sci. USA *87*, 6934–6938.

Beck, S., and Barrell, B.G. (1988). Human cytomegalovirus encodes a glycoprotein homologous to MHC class I antigens. Nature *331*, 269–272.

Biassoni, R., Pessino, A., Malaspina, A., Cantoni, C., Bottino, C., Sivori, S., Moretta, L., and Moretta, A. (1997). Role of amino acid position 70 in the binding affinity of p50.1 and p58.1 receptors for HLA-Cw4 molecules. Eur. J. Immunol. *27*, 3095–3099.

Borges, L., Hsu, M.L., Fanger, N., Kubin, M., and Cosman, D. (1997). A family of human lymphoid and myeloid Ig-like receptors, some of which bind to MHC class I molecules. J. Immunol. *159*, 5192–5196.

Boyington, J.C., Motyka, S.A., Schuck, P., Brooks, A.G., and Sun, P.D. (2000). Crystal structure of an NK cell immunoglobulin-like receptor in complex with its class I MHC ligand. Nature *405*, 537–543.

Bravo, J., Staunton, D., Heath, J.K., and Jones, E.Y. (1998). Crystal structure of a cytokine-binding region of gp130. EMBO J. *17*, 1665–1674.

Brünger, A.T., Adams, P.D., Clore, G.M., Gros, P., Grosse-Kunstleve, R.W., Jiang, J.-S., Kuszewski, J., Nilges, M., Pannu, N.S., Read, R.J., et al. (1998). Crystallography and NMR system: a new software system for macromolecular structure determination. Acta Crystallogr. D *54*, 905–921.

CCP4 (Collaborative Computational Project 4) (1994). The CCP4 suite: programs for protein crystallography. Acta. Crystallogr. D *50*, 760–763.

Chapman, T.L., Heikema, A.P., and Bjorkman, P.J. (1999). The inhibitory receptor LIR-1 uses a common binding interaction to recognize classical and non-classical class I MHC molecules and the viral MHC homolog UL18. Immunity *11*, 603–613.

Colonna, M., and Samaridis, J. (1995). Cloning of immunoglobulin-superfamily members associated with HLA-C and HLA-B recognition by human natural killer cells. Science *268*, 405–408.

Colonna, M., Navarro, F., Bellon, T., Llano, M., Garcia, P., Samaridis, J., Angman, L., Cella, M., and Lopez-Botet, M. (1997). A common inhibitory receptor for major histocompatibility complex class I molecules on human lymphoid and myelomonocytic cells. J. Exp. Med. *186*, 1809–1818.

Colonna, M., Samaridis, J., Cella, M., Angman, L., Allen, R.L., O'Callaghan, C.A., Dunbar, R., Ogg, G.S., Cerundolo, V., and Rolink, A. (1998). Human myelomonocytic cells express an inhibitory receptor for classical and nonclassical MHC class I molecules. J. Immunol. *160*, 3096–3100.

Cosman, D., Fanger, N., Borges, L., Kubin, M., Chin, W., Peterson, L., and Hsu, M.-L. (1997). A novel immunoglobulin superfamily receptor for cellular and viral MHC class I molecules. Immunity *7*, 273–282.

de Vos, A.M., Ultsch, M., and Kossiakoff, A.A. (1992). Human growth hormone and extracellular domain of its receptor: crystal structure of the complex. Science *255*, 306–312.

Fan, Q.R., Mosyak, L., Winter, C.C., Wagtmann, N., Long, E.O., and Wiley, D.C. (1997). Structure of the inhibitory receptor for human natural killer cells resembles haematopoietic receptors. Nature *389*, 96–100.

Fanger, N.A., Cosman, D., Peterson, L., Braddy, S.C., Maliszewski, C.R., and Borges, L. (1998). The MHC class I binding proteins LIR-1 and LIR-2 inhibit Fc receptor-mediated signaling in monocytes. Eur. J. Immunol. *28*, 3423–3434.

Garman, S.C., Kinet, J.P., and Jardetzky, T.S. (1998). Crystal structure of the human high-affinity IgE receptor. Cell *95*, 951–961.

Huber, A.H., Wang, Y.-M.E., Bieber, A.J., and Bjorkman, P.J. (1994). Crystal structure of tandem type III fibronectin domains from *Drosophila* neuroglian at 2.1 Å. Neuron *12*, 717–731.

Janin, J. (1997). Specific versus non-specific contacts in protein crystals. Nat. Struct. Biol. *4*, 973–974.

Karlsson, R., and Fält, A. (1997). Experimental design for kinetic analysis of protein-protein interactions with surface plasmon resonance biosensors. J. Immunol. Methods *200*, 121–133.

Kraulis, P.J. (1991). MOLSCRIPT: a program to produce both detailed and schematic plots of protein structures. J. Appl. Crystallogr. *24*, 946–950.

Lanier, L.L. (1998). NK cell receptors. Annu. Rev. Immunol. *16*, 359–393.

Lebrón, J.A., Bennett, M.J., Vaughn, D.E., Chirino, A.J., Snow, P.M., Mintier, G.A., Feder, J.N., and Bjorkman, P.J. (1998). Crystal structure of the hemochromatosis protein HFE and characterization of its interaction with transferrin receptor. Cell *93*, 111–123.

Livnah, O., Stura, E.A., Johnson, D.L., Middleton, S.A., Mulcahy, L.S., Wrighton, N.C., Dower, W.J., Jolliffe, L.K., and Wilson, I.A. (1996). Functional mimicry of a protein hormone by a peptide agonist: the EPO receptor complex at 2.8A. Science *273*, 464–471.

Maenaka, K., Juji, T., Stuart, D.I., and Jones, E.Y. (1999). Crystal structure of the human p58 killer cell inhibitory receptor (KIR2DL3) specific for HLA-Cw3-related MHC class I. Structure *7*, 391–398.

Maxwell, K.F., Powell, M.S., Hulett, M.D., Barton, P.A., McKenzie, I.F., Garrett, T.P., and Hogarth, P.M. (1999). Crystal structure of the human leukocyte Fc receptor, FcγRIIa. Nat. Struct. Biol. *6*, 437–442.

Merritt, E.A., and Murphy, M.E.P. (1994). Raster3D Version 2.0, a program for photorealistic molecular graphics. Acta Crystallogr. D *50*, 869–873.

Navarro, F., Llano, M., Bellon, T., Colonna, M., Geraghty, D.E., and Lopez-Botet, M. (1999). The ILT2(LIR1) and CD94/NKG2A NK cell receptors respectively recognize HLA-G1 and HLA-E molecules coexpressed on target cells. Eur. J. Immunol. *29*, 277–283.

Navaza, J. (1994). AMORE - an automated package for molecular replacement. Acta Crystallogr. A *50*, 157–163.

Otwinowski, Z., and Minor, W. (1997). Processing of X-ray diffraction data collected in oscillation mode. Methods Enzymol. *276*, 307–326.

Samaridis, J., and Colonna, M. (1997). Cloning of novel immunoglobulin superfamily receptors expressed on human myeloid and lymphoid cells: structural evidence for new stimulatory and inhibitory pathways. Eur. J. Immunol. *27*, 660–665.

Snyder, G.A., Brooks, A.G., and Sun, P.D. (1999). Crystal structure of the HLA-Cw3 allotype-specific killer cell inhibitory receptor KIR2DL2. Proc. Natl. Acad. Sci. USA *96*, 3864–3869.

Somers, W., Ultsch, M., De Vos, A.M., and Kossiakoff, A.A. (1994). The X-ray structure of a growth hormone-prolactin receptor complex. Nature *372*, 478–481.

Sondermann, P., Huber, R., and Jacob, U. (1999). Crystal structure of the soluble form of the human Fcγ receptor IIb: a new member of the immunoglobulin superfamily at 1.7 Å resolution. EMBO J. *8*, 1095–1103.

Sondermann, P., Huber, R., Oosthuizen, V., and Jacob, U. (2000). The 3.2 Å crystal structure of the human IgG1 Fc fragment-FcγRIII complex. Nature *406*, 267–273.

Su, X.-D., Gastinel, L.N., Vaughn, D.E., Faye, I., Poon, P., and Bjorkman, P.J. (1998). Crystal structure of hemolin: a horseshoe shape with implications for homophilic adhesion. Science *281*, 991–995.

Vales-Gomez, M., Reyburn, H.T., Mandelboim, M., and Strominger, J.L. (1998). Kinetics of interaction of HLA-C ligands with natural killer cell inhibitory receptors (erratum). Immunity *9*, 892.

Vaughn, D.E., and Bjorkman, P.J. (1997). High affinity binding of the neonatal Fc receptor to its IgG ligand requires receptor immobilization. Biochemistry *36*, 9374–9380.

Wagtmann, N., Biassoni, R., Cantoni, C., Verdiani, S., Malnati, M.S., Vitale, M., Bottino, C., Moretta, L., Moretta, A., and Long, E.O. (1995). Molecular clones of the p58 NK cell receptor reveal immunoglobulin-related molecules with diversity in both the extra- and intracellular domains. Immunity *2*, 439–449.

Wines, B.D., Hulett, M.D., Jamieson, G.P., Trist, H.M., Spratt, J.M., and Hogarth, P.M. (1999). Identification of residues in the first domain of human Fc alpha receptor essential for interaction with IgA. J. Immunol. *162*, 2146–2153.

Winter, C.C., and Long, E.O. (1997). A single amino acid in the p58 killer cell inhibitory receptor controls the ability of natural killer cells to discriminate between the two groups of HLA-C allotypes. J. Immunol. *158*, 4026–4028.

Winter, C.C., Gumperz, J.E., Parham, P., Long, E.O., and Wagtmann, N. (1998). Direct binding and functional transfer of NK cell inhibitory receptors reveal novel patterns of HLA-C allotype recognition. J. Immunol. *161*, 571–577.